Journal of Power Sources 187 (2009) 444–451

Contents lists available at ScienceDirect

Journal of Power Sources

journal homepage: www.elsevier.com/locate/jpowsour

Visualization and quantification of cathode channel flooding in PEM fuel cells

Irfan S. Hussaini, Chao-Yang Wang*

Department of Mechanical and Nuclear Engineering, and Electrochemical Engine Center (ECEC), The Pennsylvania State University, University Park, PA 16802, United States

ARTICLE INFO

Article history:
Received 3 October 2008
Received in revised form 6 November 2008
Accepted 7 November 2008
Available online 18 November 2008

Keywords:
Polymer electrolyte fuel cell
Visualization
Two-phase flow
Channel flooding
Water management
Flow map

ABSTRACT

An understanding of two-phase flow mechanisms in micro-channels is critical to water management in fuel cell applications. In this work, an in situ visualization study of cathode flooding in an operating fuel cell is presented. Gas relative humidities of 26%, 42% and 66%, current densities of 0.2, 0.5 and 0.8 A cm^{-2} and flow stoichiometries ranging from 2 to 4 are used in this study which represent typical operating conditions for automotive applications. Results are presented in the form of a flow map depicting various two-phase flow patterns. The impact of flooding is also presented in terms of measurable parameters like two-phase pressure drop coefficient and voltage loss. A new parameter called wetted area ratio is introduced to characterize channel flooding and liquid water coverage on a gas diffusion layer, and its repeatability with multiple tests is demonstrated.

1. Introduction

Hydrogen-fueled proton exchange membrane (PEM) fuel cells are considered the most promising candidates for automotive applications. Water management in PEMFCs features prominently among the list of technical challenges yet to be resolved and has received considerable attention over the past several years [1–3]. A vast majority of PEMFCs use fluorinated membranes with perfluorosulfonic acid (SO_3H^-) group due to their excellent combination of properties such as high protonic conductivity, good chemical, thermal and mechanical stability and water permeability. Protonic conductivity is the single most important property of an electrolyte membrane and it is found to be highly dependent on its degree of hydration. In an operating fuel cell, membrane hydration is affected by factors such as its thickness and morphology, gas diffusion layer, flow-field design, operating current density, gas humidification and cell temperature.

While hydration of membrane is highly desirable, presence of water in excess can be detrimental to cell performance as it leads to flooding. Flooding refers to the phenomenon of accumulation of liquid water on the electrode surface, in the gas diffusion layer (GDL) or in gas channels resulting in blockage of active electrochemical sites [4]. The cathode side is the first to be affected as it is the water generating side. Flooding causes a two-fold impact on cell performance: a drop in cell voltage and a rise in parasitic pumping power to overcome the increased pressure drop, which together result in a significant reduction in system efficiency. Proper water management is therefore crucial for optimum performance of the cell and also for enhancing membrane durability.

Development of an effective water management strategy hinges upon an understanding of two-phase flow in operating fuel cells [2,3]. Experimental work to study flooding may be broadly classified into direct and indirect methods. Direct methods utilize in situ visualization techniques using either a transparent cell [5–8] or neutron radiography [9–11] to observe the phenomena of liquid water formation and removal. Indirect techniques rely on analysis of externally measurable parameters such as pressure drop fluctuations to estimate the nature of two-phase flow [12–15]. Resident time distribution method is another indirect technique recently developed for detecting and quantifying presence of liquid water in operating fuel cells [16,17].

While numerous visualization studies on cathode-side channel flooding have been reported in literature, their outcome in general has been limited to a qualitative description of flow patterns under a given set of operating conditions. Quantitative results of two-phase flow patterns and parameters would be more desirable for fuel cell stack design and needed for experimental validation of multi-physics computational models that account for two-phase interactions in gas channels.

The objective of this paper is to present results from an in situ visualization study of cathode-side flooding with the help of channel images and to present the information in the form of a flow map. Results are quantified in terms of two-phase pressure

* Corresponding author. Tel.: +1 814 863 4762; fax: +1 814 863 4848.
E-mail address: cxw31@psu.edu (C.-Y. Wang).

0378-7753/$ – see front matter © 2008 Elsevier B.V. All rights reserved.
doi:10.1016/j.jpowsour.2008.11.030

Nomenclature

A_c	cross-sectional area of each channel (m^2)
A_m	effective MEA area (m^2)
F	Faraday's constant, 96,487,000 C $kmol^{-1}$
i	current density (A m^{-2})
L_{tot}	channel length (m)
$\dot{m}_w$	mass flow rate of water (kg s^{-1})
M	molecular weight (kg $kmol^{-1}$)
N	number of channels
P	fuel cell operating pressure (kPa)
P_{sat}	saturation pressure of water (kPa)
ΔP	pressure drop (Pa)
$RH_{c,in}$	relative humidity at cathode inlet
U_g^s, U_l^s	superficial gas and liquid phase velocities (m s^{-1})
ΔV	voltage loss (mV)

Greek letters

α	net water flux per proton flux
ϕ_1	wetted area ratio
ϕ_{2p}	two-phase pressure drop coefficient
ρ	density (kg m^{-3})
ζ	flow stoichiometry

drop coefficient, voltage loss and a flooding parameter called wetted-area ratio on the surface of GDL.

2. Experimental setup and test conditions

2.1. Optical fuel cell

A picture of the optical fuel cell mounted on its test stand is shown in Fig. 1. A straight-channel cell with an effective membrane area of 14 $cm^2$is used in this study. More detail of the optical cell construction can be found in [6,8]. The MEA consists of a 30 μm thick Gore membrane sandwiched between 10 μm thick catalyst layers. A 200 μm thick Toray carbon paper coated with a 30 μm micro-porous layer (MPL) forms the GDL. Both GDL and MPL are loaded with PTFE for imparting hydrophobicity to their structures. Bipolar plates consist of 0.5 mm thick, gold-coated stainless steel plates with seven evenly spaced flow channels of size 10 cm × 1 mm × 0.5 mm. Bipolar plates and Lexan plate are left untreated and are therefore hydrophilic in nature. The flow field is identical on the anode and cathode sides.

The cathode side is covered by a transparent Lexan plate providing a clear view of the channels. Thermostat-controlled external heating is used to maintain the cell at constant temperature. The cathode side is heated using cartridge-type electrical heaters placed in a metallic plate over the Lexan, while the anode side is heated using water circulated from a constant temperature bath. Heat capacitance of the bulk assembly is much higher than that of the MEA thus ensuring an isothermal environment within the cell. High purity hydrogen and breathing quality air are used as the reactants.

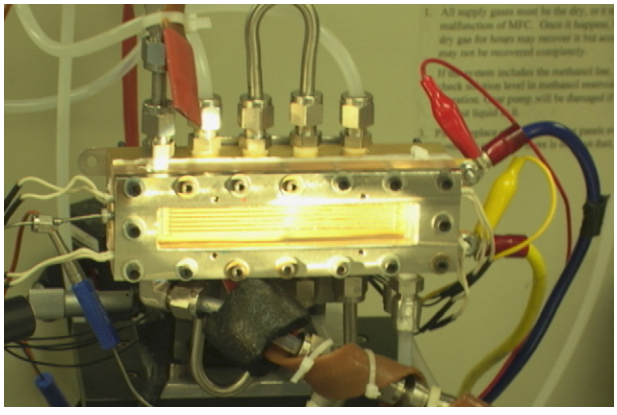

Fig. 1. A picture of the transparent PEM fuel cell used in this study.

2.2. Test setup and instrumentation

The testing equipment consists of a Teledyne Fuel Cell Test Station, together with a high resolution Olympus video microscope for capturing images. The test station is capable of controlling fuel and oxidant flow rates and their humidification levels, cell temperature and back pressure with the help of computer-based software. A Rosemount pressure transducer is used for pressure measurements across the cathode channels. The pressure transducer has an accuracy of ±10 Pa. All data acquisition is done at a sampling interval of 1 s. Membrane high-frequency resistance (HFR), a primary indicator of membrane water content, is measured with an Agilent AC milli-ohm meter at a frequency of 1 kHz. Further details of this technique for electrolyte resistance measurement are available in [18,19].

2.3. Test conditions

Tests are conducted at cell temperature of 80° C and at gas humidification levels of 66%, 42% and 26%. Current densities of 0.8, 0.5 and 0.2 A $cm^{-2}$and flow stoichiometries of 4, 3.5, 3, 2.5 and 2 are used. In all the above cases, the cell is maintained at a constant temperature of 80° C and a back-pressure of 1 atm (gauge). Counterflow configuration and equal anode and cathode flow stoichiometries are used. At a given current density, mass flow rates of hydrogen and air are obtained from the definition of stoichiometry given by

$$\zeta_a = \frac{\dot{m}_{H_2}}{M_{H_2}(iA_m/2F)} \qquad \zeta_c = \frac{\dot{m}_{air}}{2.38M_{air}(iA_m/2F)} \tag{1}$$

3. Results and discussion

3.1. Channel images

Channel images are recorded at regular intervals to monitor build-up of liquid water in the channels. In this paper, for purpose of brevity, only a limited set of steady-state images taken after 30 min of operation is shown. All images show the cathode side, with air flowing from right-to-left.

Fig. 2 shows cathode channel images at 66% RH, 0.8 A cm^{-2} and at stoichiometries of 4 and 2. It is seen that at stoichiometry of 4, barely a few liquid droplets accumulate in the top-most channel whereas at stoichiometry of 2, liquid water is found to cover a considerable area in the channels existing in the form of droplets, film and slugs. Over the range of stoichiometries studied, the amount of liquid water and its spatial distribution has been observed to be different in each channel. In all cases, however, flooding is found to be concentrated near the exit region and the dry-to-wet transition front is found to move upstream as the stoichiometry is lowered. The top and bottom channels are found to accumulate more water as compared to other channels. This was shown from simulation studies to be due to GDL intrusion and subsequent flow mal-distribution [20]. During cell assembly, the GDL material is compressed only under the ribs of the bi-polar plate, whereas the material under the channel remains un-compressed and tends to intrude into the channel. Moreover, the compression and hence the intrusion is more pronounced in the channels near the edges than

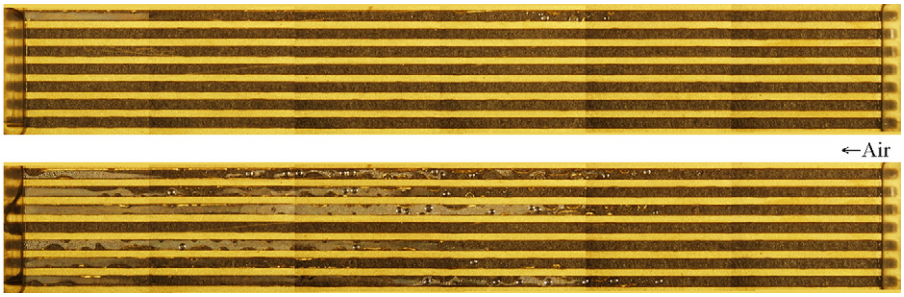

Fig. 2. Images showing liquid water in cathode channels at 0.8 A cm^{-2}, 66% RH and stoichiometries of 4 (above) and 2 (below) respectively.

in those near the centre. As a result, the flow area in the end channels is slightly lower than the rest. To maintain equal pressure drop across all channels, the flow velocity decreases in the end channels and increases in others. As a result of such a mal-distribution of flow, more water gets accumulated in the top and bottom channels than in others.

Fig. 3 shows channel images under a relatively dry gas flow with 26% RH, and at current density of 0.8 A cm^{-2}. Liquid water is observed only at stoichiometries of 2.5 and below. It is seen that even with low RH gas, liquid water flooding occurs at low stoichiometry conditions. This is because at constant stoichiometry, a low current density results in a low gas flow rate which is insufficient to remove liquid water. Thus, the level of flooding is higher at low flow rate conditions such as low current densities and stoichiometries and negates the theoretically high efficiencies expected at these conditions.

3.2. Flow map

An attempt is made to synthesize the numerous channel images in the form of a flow map that may be used to display the entire spectrum of flow patterns observed and also to predict two-phase flow patterns based on operating conditions. Two-phase flow in micro-channels in PEMFCs is complicated due to features unique to fuel cells such as in situ generation of liquid water and its influx into the flow channel, presence of porous GDL wall, bounding walls with different wetting characteristics, evaporation of water into the gas stream and internal transport of water between anode and cathode sides. Moreover, presence of multiple channels leads to a non-uniformity in two-phase flow patterns among channels.

As also reported in other studies [6,7,8], two-phase transport in fuel cell micro-channels is found to occur principally in the form of droplet, film and slug-flow with the two-phase region being preceded by a single-phase region. A brief description of the different flow patterns as observed from channel images is given below. Actual images corresponding to these flow patterns are given in Fig. 4.

1. Single-phase flow: In this regime, hardly any water droplets are observed on the GDL surface and the flow is mostly in the form of partially humidified gas. Water droplets may appear sporadically on the GDL surface but tend to be quickly evaporated by the flowing air stream.
2. Droplets: This region is dominated by water droplets that emerge from underneath the GDL surface and remain adhered to the surface by surface tension forces. Mass transfer occurs at the interface with the flowing gas. Due to hydrophobic nature of carbon paper GDL surface, droplets are circular in shape and do not spread out laterally on the surface. The maximum radius a droplet can grow to is limited either by its detachment size (under shearing action by gas flow) or the channel depth which is 0.5 mm in this case.
3. Film flow: Further downstream, the influx of liquid water through GDL is sufficiently high so that the droplets, on contact either with neighboring droplets or channel walls, coalesce and are wicked into the walls and form a liquid film of growing thickness. A wavy motion is observed on the film surface due to the continuous influx of water and coalescence of droplets. Large droplets are no longer observed. Tiny droplets may appear and are generally confined to a narrow region at the centre of the channel.
4. Slug flow: Further growth of the film causes it to accumulate into a slow-moving slug. This results in oscillations in pressure drop and causes an internal adjustment of flow rate among the channels. Clogging of channels may occur when the slugs stagnate near the exit region of a channel and completely stop gas flow through it.

Flow maps are generally used for representing internal two-phase flows and are usually plotted in terms of superficial phase velocities [21,22]. Superficial velocity is defined as the bulk velocity of the phase based on the flow area of the channel and hence prior knowledge about the flow rate of each phase is needed for its estimation.

Gas superficial velocity is defined here at the "inlet" based on mass flow rate of air entering the cell and is given by

$$U_{\mathrm{g}}^{\mathrm{s}} = \frac{1}{N\rho_{\mathrm{air}}A_{\mathrm{c}}}\left[2.38\zeta\frac{M_{\mathrm{air}}iA_{\mathrm{m}}}{2F}\right] \tag{2}$$

In fuel cells, generation of liquid phase occurs internally and factors such as internal transport between anode and cathode sides by back-diffusion and electro-osmotic drag, partial evaporation of liquid into the gas phase and stoichiometric consumption of a component of gaseous phase (O_2 in air) further complicate the situation. Therefore, a precise determination of superficial velocity of the liquid phase is difficult to achieve. However, a superficial velocity for the liquid phase may be defined at the "exit" in terms of net liquid water production rate in the cell and assuming a saturated exhaust, as

$$U_{\mathrm{l}}^{\mathrm{s}} = \frac{1}{N\rho_{\mathrm{H_2O}}A_{\mathrm{c}}}\left[\dot{m}_{\mathrm{w,prod}} - \dot{m}_{\mathrm{w,evap}}\right] \tag{3}$$

where

$$\dot{m}_{\mathrm{w,prod}} = (1+2\alpha)\frac{M_{\mathrm{H_2O}}iA_{\mathrm{m}}}{2F} \tag{4}$$

$$\dot{m}_{\mathrm{w,evap}} = \frac{M_{\mathrm{H_2O}}iA_{\mathrm{m}}}{2F}\left[(2.38\zeta - 0.5)\frac{P_{\mathrm{sat}}}{P - P_{\mathrm{sat}}} - 2.38\zeta\frac{P_{\mathrm{sat}}\mathrm{RH}_{\mathrm{c,in}}}{P - P_{\mathrm{sat}}\mathrm{RH}_{\mathrm{c,in}}}\right] \tag{5}$$

It may be noted from its definition that local liquid superficial velocity is zero at the channel inlet, increases linearly with water generation rate and reaches a value of $U_{\mathrm{l}}^{\mathrm{s}}$ at the channel exit. The

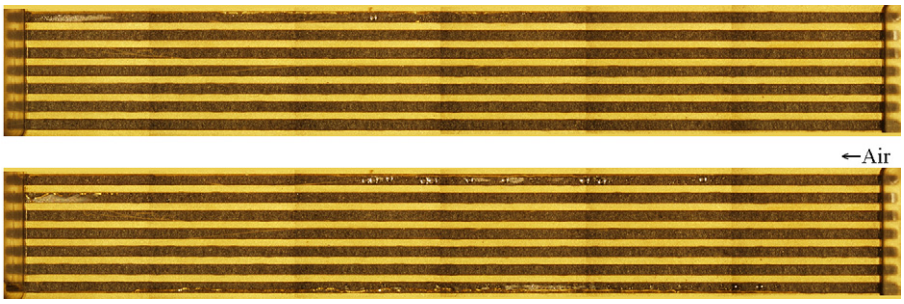

Fig. 3. Flooding in cathode channels at 0.8 A cm^{-2}, 26% RH and stoichiometries of 2.5 (above) and 2 (below) respectively (no liquid water is observed at $\zeta \geq 3$).

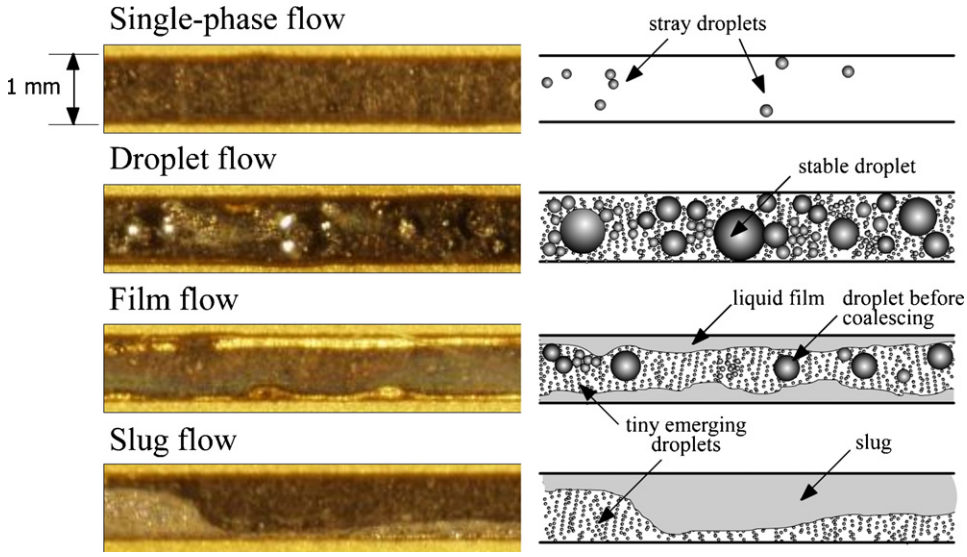

Fig. 4. Magnified view of flow patterns in channels and their corresponding line illustrations showing the form and distribution of liquid water.

value of α, the net water transport coefficient, varies with operating conditions as well as GDL/MPL dimensions and properties [23]. However, for the sake of convenience, it is assigned a constant value of 0.1 in Eq. (4).

Flow patterns observed from channel images are presented in the form of a flow map in Fig. 5. Equations of curve-fitted lines separating the slug-flow and single-phase regions are also shown. For plotting the data, channel image is divided into several segments and dominant flow pattern in each segment is identified by visual inspection. Gas phase velocity is obtained from Eq. (2) whereas the local superficial liquid phase velocity, which depends on the cumulative amount of water produced, is calculated by scaling U_l^s with respect to the segment location along the length of the cell. The observed flow pattern is then marked on the flow map corresponding to these velocities.

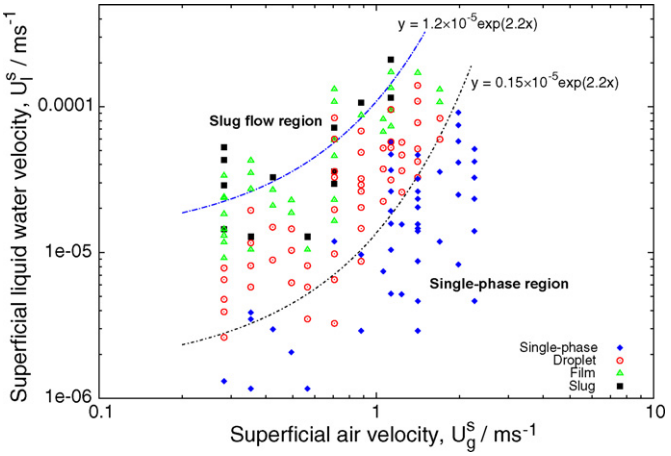

Fig. 5. Flow map of cathode channel flooding on hydrophobic GDL surface.

The flow map thus obtained may be used to extract information such as the threshold velocity for transition from single-phase gaseous flow to two-phase flow, the location of transition, and the flow pattern at a given location in the channel. The flow patterns presented here are for typical hydrophobic carbon paper GDL, details of which are given in Section 2. Threshold velocities obtained from flow map can be used to design the flow field and to determine system operating parameters for minimizing channel flooding. This information may also be utilized in the validation of channel two-phase flow models.

3.3. Two-phase pressure drop coefficient

Pressure drop is a readily measurable parameter that may be used to quantify channel flooding. In this study, pressure drop across the cathode side is recorded in real time to determine the effect of water build-up. Pressure drop over a two-phase region is expressed here by a coefficient ϕ_{2p} defined as

$$\phi_{2p} = \frac{\Delta P_{\text{actual}}}{\Delta P_{\text{single-phase}}} \tag{6}$$

The actual pressure drop (ΔP_{actual}) is the value recorded by the pressure transducer during fuel cell operation and it includes the effect of occurrence of liquid water, if any, in gas channels. The

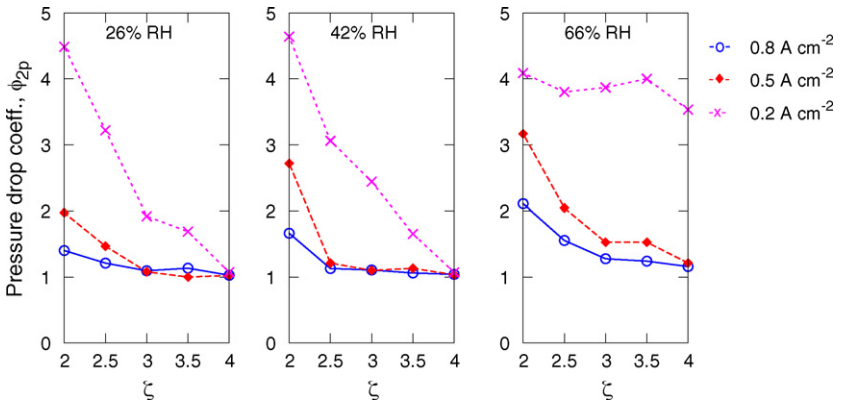

Fig. 6. Two-phase pressure drop coefficient on cathode side.

term $\Delta P_{\text{single-phase}}$ represents the mean value of pressure drop measured during an open-circuit period when gases are flowing at their respective stoichiometries and a single-phase, gaseous flow exists in the cell. The cell is purged of all liquid water before making this measurement. Thus, a value of unity for the coefficient ϕ_{2p} indicates absence of liquid water in the cell. Due to the dynamic nature of liquid water formation and removal, pressure drop does not always reach a steady-state value. Hence, an average value of pressure drop over a 2-min interval following a 25-min period of operation is determined and the pressure drop coefficient is calculated using this value.

Fig. 6 shows the computed two-phase pressure drop coefficient at the various operating conditions considered. At a stoichiometry of 4, using dry gases with 26% RH and the three levels of current density, ϕ_{2p} is about unity indicating absence of liquid water in the cell. In contrast, at a higher humidity condition of 66% RH, current density of 0.2 A cm^{-2} and a stoichiometry of 4, ϕ_{2p} is about 3.5 indicating a substantial presence of liquid water in the fuel cell. At other operating conditions too, the impact of liquid water presence on fuel cell performance is clearly demonstrated through the pressure drop coefficient. Results thus show that a three- to four-fold increase in pressure drop can result due to channel flooding, particularly at low stoichiometries and current densities, irrespective of gas RH.

3.4. Voltage loss due to flooding and membrane HFR

Occurrence of liquid water in the cell causes blockage of reactant transport to the electrode surface, causing deterioration in cell voltage under constant load conditions. The impact of flooding can be measured in terms of the magnitude of voltage loss. Fig. 7 shows the average voltage loss over a 2-min period following a 25 min operation. At conditions which do not favor flooding such as high current density and stoichiometry, there is minimal voltage loss and a steady, optimum voltage is achieved from the cell. However, under conditions leading to electrode and channel flooding, voltage loss increases and is found to be as high as 60–80 mV under stoichiometry of 2 and current densities of 0.5 and 0.2 A cm^{-2}. Under conditions of severe flooding, cell voltage is found to fluctuate erratically due to formation of high-frequency water slugs in gas channels leading to an occasional cell shut-down.

Table 1
Average values of HFR after 25 min of operation for representative test conditions.

Gas RH (%)	Current density, i (A cm^{-2})	HFR (m Ω cm^2)				
		$\zeta = 4$	$\zeta = 3.5$	$\zeta = 3$	$\zeta = 2.5$	$\zeta = 2$
66	0.8	111	100	95	108	104
	0.2	96	91	99	96	94
42	0.8	117	110	110	105	103
	0.2	118	112	110	109	111

Referring to Fig. 7, the data point corresponding to 66% RH, 0.5 A cm^{-2} and stoichiometry of 4 shows a deviation from the trend. This irregularity is due to wide fluctuations in cell voltage caused by liquid water formation and removal which, in this case, do not reach a steady-state over the interval in which the average is computed.

Membrane HFR is another parameter that provides good insight into the state of hydration of the membrane under steady-state operation. Table 1 lists the mean values of HFR over a 2-min interval after 25 min of operation for some representative test conditions. HFR values are found to be higher at higher current densities and

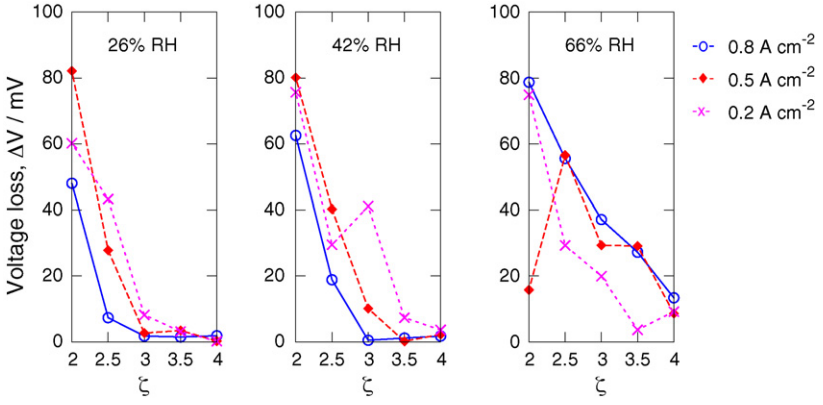

Fig. 7. Loss in cell voltage due to channel flooding.

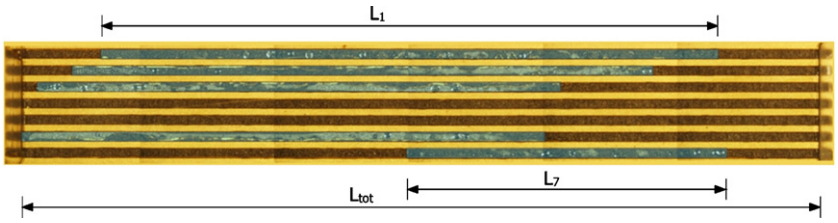

Fig. 8. Image showing extent of liquid water region in different channels.

stoichiometries. This is due to insufficient membrane hydration caused by an increased rate of net water transport from anode to cathode leading to a drier membrane on the anode side, and also by an increased rate of water removal from the cathode side caused by higher gas flow. HFR values read in conjunction with cell-voltage, pressure drop data and channel images indicate that a low but steady HFR reading accompanied with rapid fluctuations in cell voltage is an important sign of channel flooding.

3.5. Wetted area ratio

Based on images presented earlier, it is observed that the amount of liquid water in the cell is found to be randomly distributed across channels. In order to account for this spatial distribution of liquid water in channels, a new parameter called wetted area ratio (ϕ_1) is introduced. It is defined as the fraction of the total channel surface area covered by liquid water given by

$$\phi_1 = \frac{\text{wetted area}}{\text{total area}} \tag{7}$$

Wetted area ratio represents the total area in the channels occupied by consistent two-phase activity in the form of droplets, film or slugs so that $1 - \phi_1$ represents absolute dry single-phase region in the cell. Presence of stray and short-lived droplets is not considered in the estimation. The spacing between the droplets in the two-phase region is generally small so that they are assumed to be continuously distributed over the surface so that ϕ_1 is calculated from the ratio of wetted length to the total channel length.

Fig. 8 shows a sample image indicating the liquid water regions in different channels. The wetted region is highlighted in a transparent blue color. After identifying the wetted regions, their corresponding lengths are determined and the wetted area ratio calculated as:

$$\phi_1 = \frac{1}{NL_{\text{tot}}} \sum_{i=1}^{N} L_i \tag{8}$$

where L_i represents the wetted length in channel i.

Fig. 9 shows a plot of wetted area ratio at different current densities and stoichiometries. It is seen that at every combination of gas humidification and current density, there is a certain threshold stoichiometry above which there is no liquid water present in the gas channels. Below this threshold value, liquid water accumulation occurs and tends to increase proportionately with a decrease in stoichiometry.

It is seen from Fig. 9 that at a given stoichiometry, an increase in current density leads to a decrease in the GDL surface area covered by liquid water. Although the water production rate is higher at higher current densities, but due to correspondingly higher gas flow rates any liquid water appearing in the channels is quickly carried away from the cell either by evaporation or by flow inertia. The effect of gas RH is also evident from this figure.

Wetted area ratio is a novel parameter introduced in this study for presenting the accumulation of liquid water in gas channels in a quantitative manner. As the flooding in fuel cell micro-channels is a phenomenon governed by several operational parameters and has a certain degree of randomness associated with it, it is essential that this parameter be able to quantify the phenomena and represent it in a repeatable manner. In order to test its repeatability, a subset of experiments were repeated and the wetted area ratio re-calculated and compared.

Fig. 10 shows images from two such tests performed under identical operating conditions. It is seen that the distribution of liquid water is quite different in the two cases. However, the calculated values of ϕ_1 are found to be approximately equal. Another set of images is shown in Fig. 11 for a different set of operating conditions. In this case too, the distribution of liquid water is different but the calculated value of ϕ_1 is approximately the same.

Comparison of ϕ_1 values for all the repeated experiments is shown in Fig. 12. It is seen that except for 2 out of a total of 18 cases considered, the parameter ϕ_1 is found to be repeatable within 5% of its value. Physical distribution of liquid water across channels tends to be random in nature and may not be identical for any two experiments conducted under same test conditions. But the fact that the value of ϕ_1 turns out to be the same indicates that the water present in the channels in

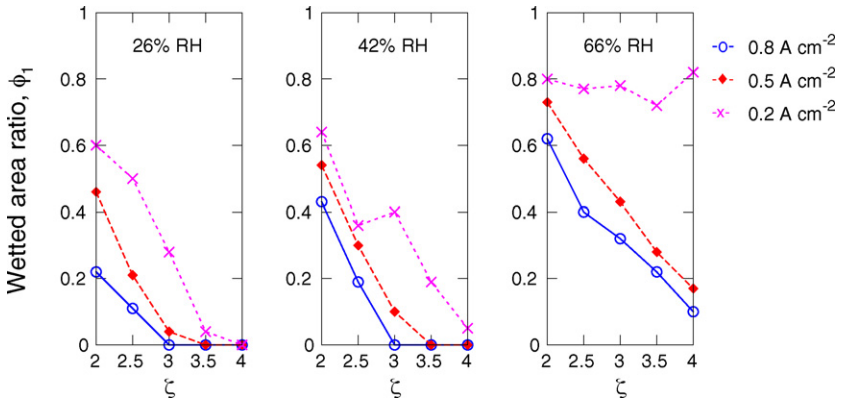

Fig. 9. Variation of calculated wetted area ratio (ϕ_1) with current density, stoichiometry and gas RH.

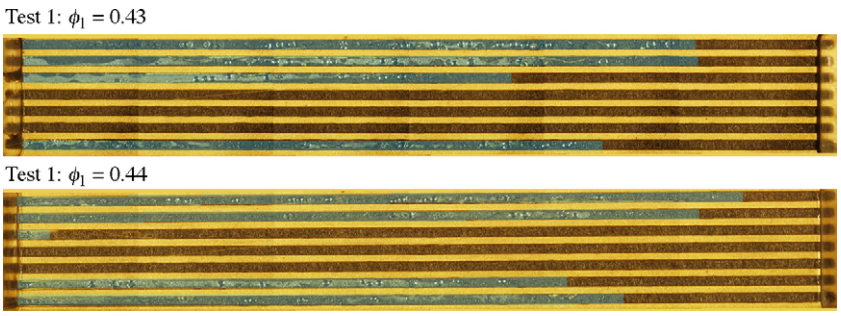

Fig. 10. Channel images from two different tests at identical test conditions of 0.8 A cm^{-2}, 42% RH and ζ = 2.

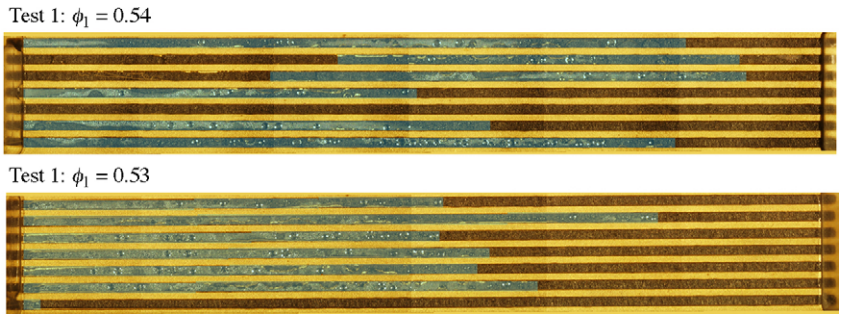

Fig. 11. Channel images from two tests at conditions of 0.5 A cm^{-2}, 42% RH and $\zeta = 2$.

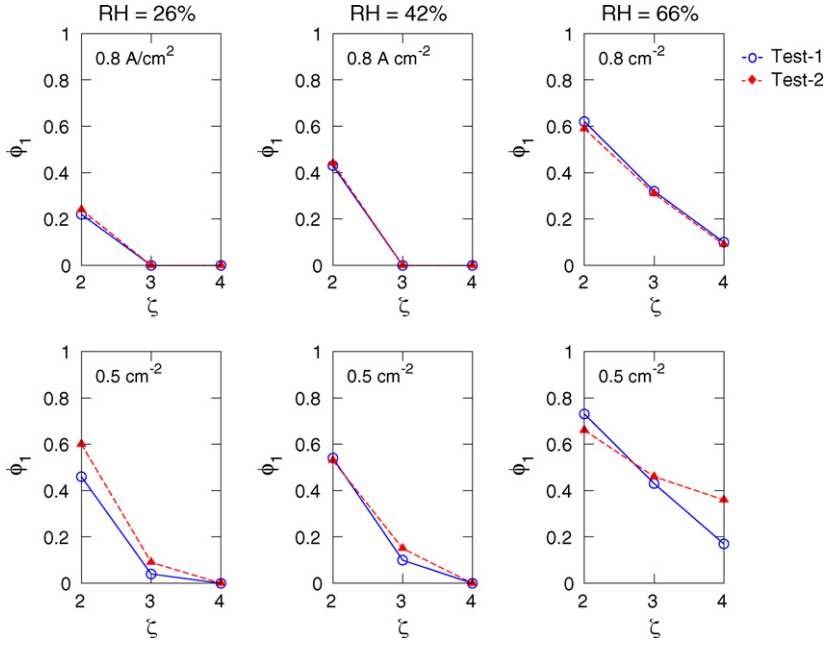

Fig. 12. Comparison of ϕ_1 values from two different test runs, at identical operating conditions.

steady-state conditions is approximately constant under given test conditions.

Wetted area ratio thus determined represents the fraction of exposed GDL surface area that is covered by liquid water. It serves as a useful parameter for validating simulation results by comparing saturation at GDL/channel interface with actual experimental data and serves as a basis for comparing effectiveness of GDL materials and structures. It may be noted that manual demarcation of wetted area involves an inherent error and uncertainty. Software-based image processing techniques capable of identifying and measuring water-covered area in channels will certainly help improve accuracy.

4. Conclusions

Visualization study of cathode side liquid water in straight channels has been carried out for a range of humidification levels, current densities and stoichiometries representing typical automotive conditions. An attempt has been made to present the findings in the form of a flow map and also quantitatively in terms of two-phase pressure drop coefficient, voltage loss and wetted area ratio. Following are the main conclusions drawn from this study.

1. Cathode GDL and channel flooding is a persistent phenomenon accompanying fuel cell operation even under low humidity con-

ditions. In most cases, flooding is found to be significant enough to cause substantial loss of cell performance. Operating conditions of low current density and low stoichiometry are found to be particularly susceptible to severe flooding under all humidity conditions considered.

2. At a given current density, the two-phase front is found to move upstream toward inlet as flow stoichiometry decreases with other factors remaining constant. The location of the front physically corresponds to the point at which cathode gas RH reaches 100%.
3. Observed flow patterns are represented in the form of a flow map, possibly the first such representation for two-phase flow in fuel cell channels. The flow map shows the spectrum of flow patterns and conditions leading to transition from one flow regime to another.
4. A two- to five-fold increase in pressure drop has been observed as a result of channel flooding. It represents a significant penalty in terms of parasitic power spent in driving reactant gases through a flooded cell.
5. Occurrence of liquid water flooding has been shown to cause a voltage drop of up to 80 mV under low stoichiometry conditions. This represents a huge loss in performance considering that a ten-fold increase in the reaction current density on electrode surface translates into a voltage increase of only about 66 mV.
6. Occurrence of rapid fluctuations in cell voltage together with a low and constant membrane HFR is characteristic of channel flooding.
7. The GDL surface area covered by liquid water may be quantified by the parameter called wetted area ratio. Actual distribution of water is found to vary from channel to channel and from experiment to experiment, but the total amount of liquid water resident in all the channels is found to be fairly constant under a given set of operating conditions.
8. Wetted area ratio is found to be repeatable within an experimental margin of uncertainty, thus indicating that it represents the state of the fuel cell at given test conditions. Its repeatability under a number of test cases has been demonstrated.

Acknowledgement

We acknowledge industrial sponsors of ECEC for financial support of this work.

References

[1] L. Carrette, K.A. Friedrich, U. Stimming, Fuel Cells 1 (2001) 5–39.
[2] C.Y. Wang, Chem. Rev. 104 (2004) 4727–4766.
[3] T.F. Fuller, J. Newman, J. Electrochem. Soc. 140 (1993) 1218–1225.
[4] U. Pasaogullari, C.-Y. Wang, J. Electrochem. Soc. 152 (2005) A380–A390.
[5] A. Theodorakakos, T. Ous, M. Gavaises, J.M. Nouri, N. Nikolopoulos, H. Yanagihara, J. Colloid Interface Sci. 300 (2006) 673–687.
[6] X.G. Yang, F.Y. Zhang, A.L. Lubawy, C.-Y. Wang, Electrochem. Solid State Lett. 7 (2004) A408–A411.
[7] H.-S. Kim, T.-H. Ha, S.-J. Park, K. Min, M. Kim, Proceedings of 3rd International ASME Conference on Fuel Cell Science, Engineering and Technology, FUELCELL2005, Ypsilanti, Michigan, May 23–25, 2005, pp. 1–7.
[8] F.Y. Zhang, X.G. Yang, C.-Y. Wang, J. Electrochem. Soc. 153 (2006) A225–A232.
[9] R.J. Bellows, M.Y. Kin, M. Arif, A.K. Thompson, D. Jacobson, J. Electrochem. Soc. 146 (1999) 1099–1103.
[10] D. Kramer, J. Zhang, R. Shimoi, E. Lehmann, A. Wokaun, K. Shinohara, G.G. Scherer, Electrochim. Acta 50 (2005) 2603–2614.
[11] M.A. Hickner, N.P. Siegel, J.S. Chen, D.N. McBrayer, D.S. Hussey, D.L. Jacobson, M. Arif, J. Electrochem. Soc. 153 (2006) A902–A908.
[12] M.W. Wambsganss, J.A. Jendrzejczyk, D.M. France, Int. J. Multiphase Flow 17 (1991) 327–342.
[13] D. Barnea, O. Shoham, Y. Taitel, Int. J. Multiphase Flow 6 (1980) 387–397.
[14] O.C. Jones, N. Zuber, Int. J. Multiphase Flow 2 (1975) 273–306.
[15] N.K. Tutu, Int. J. Multiphase Flow 8 (1982) 443–447.
[16] J. St-Pierre, J. Electrochem. Soc. 154 (2007) B724–B731.
[17] J. Diep, D. Kiel, J. St-Pierre, A. Wong, Chem. Eng. Sci. 62 (2007) 846–857.
[18] F.N. Buchi, A. Marek, G.G. Scherer, J. Electrochem. Soc. 142 (1995) 1895–1901.
[19] K.R. Cooper, M. Smith, J. Power Sources 160 (2006) 1088–1095.
[20] Y. Wang, S. Basu, C.-Y. Wang, J. Power Sources 179 (2008) 603–617.
[21] V.P. Carey, Liquid–Vapor Phase-Change Phenomena, Hemisphere Publishing Corp., Washington, DC, USA, 1992.
[22] A. Faghri, Y. Zhang, Transport Phenomena in Multiphase Systems, Elsevier Academic Press, Burlington, MA, USA, 2006.
[23] U. Pasaogullari, C.-Y. Wang, K.S. Chen, J. Electrochem. Soc. 152 (2005) A1574–A1582.